

Provided for non-commercial research and education use.  
Not for reproduction, distribution or commercial use.



This article appeared in a journal published by Elsevier. The attached copy is furnished to the author for internal non-commercial research and education use, including for instruction at the authors institution and sharing with colleagues.

Other uses, including reproduction and distribution, or selling or licensing copies, or posting to personal, institutional or third party websites are prohibited.

In most cases authors are permitted to post their version of the article (e.g. in Word or Tex form) to their personal website or institutional repository. Authors requiring further information regarding Elsevier's archiving and manuscript policies are encouraged to visit:

<http://www.elsevier.com/authorsrights>

Contents lists available at [SciVerse ScienceDirect](http://SciVerse.ScienceDirect.com)

## Aerospace Science and Technology

[www.elsevier.com/locate/aescte](http://www.elsevier.com/locate/aescte)

## Optimization of a flight-worthy scramjet combustor through CFD

P. Manna, Malsur Dharavath, P.K. Sinha, Debasis Chakraborty\*

Directorate of Computational Dynamics, Defence Research and Development Laboratory, P.O. Kanchanbagh, Hyderabad 58, India

## ARTICLE INFO

## Article history:

Received 25 February 2012

Received in revised form 16 July 2012

Accepted 25 July 2012

Available online 4 August 2012

## Keywords:

Scramjet combustor

CFD

Optimisation

## ABSTRACT

Reacting flow simulations are carried out for different fuel injection schemes and strut arrangements to obtain an optimized performance of a flight sized hydrocarbon fueled scramjet combustor using commercial CFD software. Three-dimensional Reynolds Averaged Navier–Stokes (RANS) equations are solved along with  $k-\epsilon$  turbulence model to analyse the flow field. Eddy Dissipation Model (EDM) with fast rate chemical kinetics and Lagrangian Particle Tracking Method (LPTM) are used for modeling combustion and to simulate the trajectory of the kerosene droplets. It was found that at the exit plane, considerable amount of unburnt kerosene vapour in the core regions and unused oxygen in the side wall regions are present in the baseline combustor. Modified fuel injection scheme and modified strut locations are found to improve the thrust and combustion efficiency by 18.3% and 18.6% respectively compared to the baseline configuration.

© 2012 Elsevier Masson SAS. All rights reserved.

## 1. Introduction

Development of an efficient hypersonic air breathing propulsion system for civil and military applications has driven the development of scramjet engine form early 1960s [10,24,32]. Both hydrogen and kerosene were studied extensively [6] for the fuel requirement of the scramjet engine; hydrogen for space applications and hydrocarbon fuel for air-launched missiles. Although, hydrogen is attractive because of higher specific impulse and better ignition characteristics, higher energy density and easier handling issue make liquid hydrocarbons as an attractive candidate for fuelling the scramjet engine in the lower hypersonic ( $M < 8$ ) flight regimes. Atomization, vaporization, mixing and slow chemical reactions are some of the major technical and scientific problems in the realization of liquid hydrocarbon based scramjet engine. A deeper penetration of fuel into a supersonic air stream is required for better mixing which is a key to sustained combustion. The penetration of liquid jet is studied [9] for varying dynamic pressure ratios of two streams and different droplet sizes. The typical penetration depth of the fuel jet is about 10 to 15 mm for a practical scramjet combustor in the flight region of Mach 6.0–7.0. Reaction occurs only in a small fraction of the flow field adjacent to the wall when the fuel is injected from the combustor wall [1, 33]. Therefore, not all of the oxygen supplied by air stream entering into combustor can participate in the heat release process. Furthermore, the reaction zone close to the wall will exert excessive thermal loads on the structure of the combustor. The problem of slow lateral fuel transport in the air stream can be circumvented

by injecting the fuel in the core region of the flow by means of struts and or pylons. The oblique shocks generated from the struts also augment the mixing which is very much needed in high speed propulsion devices.

Fuel injection from the struts has been experimented upon in some subscale scramjet engine including airframe integrated scramjet module [23,30]. The subscale scramjet engine being developed at NAL, Japan [30] uses the fuel injection strut to improve mixing. Scramjet engines with struts were tested at Engine Test Facilities for Mach 4, 6 and 8 conditions [14,15,30]. Reported experimental and numerical studies [4,11,12,17,22,34,35] on hydrocarbon fueled supersonic combustion mostly address the issues of cavity based flame holder and injection system in laboratory scaled combustor. The penetration of liquid fuel in supersonic flow is critical in any practical scramjet combustor. The studies on strut-based scramjet combustor with kerosene fuel are highly limited. Vinogradov et al. [31] conducted experimental investigations to determine the ignition, piloting, and flame holding characteristics in a scramjet combustor operating on kerosene. In order to improve the fuel distribution and mixing with supersonic air flow, kerosene was injected from the strut located in the middle of the duct. Stable combustion of kerosene was achieved even after turning off pilot hydrogen. Bouchez et al. [3] carried out experimental investigations of hydrocarbon fueled scramjet under EADS Aerospaiale Matra Missile (AMM) internal research program at Bourges Le Subdray test facility. Two identical metallic water-cooled and liquid kerosene-cooled struts were used for the fuel injection in the combustor. To ensure ignition, gaseous hydrogen was used as pilot fuel at the base of the struts. Kerosene equivalence ratio was varied from 0 to 1.0. Various flow parameters (wall pressure, wall heat flux, total temperature at combustor exit, thrust, etc.) were

\* Corresponding author.

E-mail address: [debasis\\_cfd@drdl.drdo.in](mailto:debasis_cfd@drdl.drdo.in) (D. Chakraborty).

**Nomenclature**

$A_{ebu}, B_{ebu}$	Model coefficient of EDM	$R_{k,EDM}$	Mixing rate of EDM
$D$	Particle diameter	SMD	Sauter mean diameter
EDM	Eddy Dissipation Model	$T$	Temperature
$f$	Parameter of GCI	$W$	Width of the combustor
$F_s$	Factor of safety in GCI	$X, Y, Z$	Three axes direction
GCI	Grid convergence ratio	$y$	Mass fraction
$h$	Grid spacing		
$H$	Height of the combustor	<b>Symbol</b>	
$k$	Turbulent kinetic energy	$\gamma$	Measure of particle size distribution
$L$	Length of the combustor, also left side of the combustor	$\eta$	Combustion efficiency
LPTM	Lagrangian Particle Tracking Method	$\varepsilon$	Turbulent kinetic energy dissipation rate
$M$	Mach number	$\in$	Relative difference of $f$
$p$	Order of accuracy in GCI		
$P$	Pressure	<b>Subscript</b>	
$r_k$	Stoichiometric ratio	$i, out$	Inlet, outlet
$R$	Right side of the combustor	$f, ox, p$	Fuel, oxidizer, product
RANS	Reynolds averaged Navier–Stokes	1, 2	Fine and coarse grid
$R_c$	Cumulative mass fraction above a particle diameter $D$	$o$	Total condition of a flow

measured. Optical methods including passive spectroscopy were also used to characterize the flow. The experimental results were used to validate the CFD codes for the prediction of kerosene fueled scramjet combustor flow field.

With the advent of powerful computer and robust numerical algorithm, CFD is complementing ‘difficult to perform’ experiment and thus playing a major role in developing a comprehensive understanding of the key phenomenon that dominate performances. To accurately model scramjet flow field, CFD must adequately resolve several complex physical processes including three-dimensionality, shock boundary interaction, turbulent mixing of high speed streams, atomization and combustion of liquid fuel. Numerical studies for scramjet combustor with kerosene fuel are highly limited in the literature. Refs. [3] and [8] describe earlier numerical studies on strut-based kerosene fuelled scramjet combustor. They have used MSD-2.2.2 CFD code developed at ONERA for the prediction of the flow inside kerosene fuelled scramjet combustor with strut-based injection system. Chemical reactions and combustion models for both hydrogen and kerosene fuel are used in their reactive flow calculation. Although they have mentioned the use of nonreactive two-phase simulation with liquid droplet for selecting the injector location; enough details are not provided for two-phase reactive calculations. A reasonably good match is obtained between the computational and experimentally measured wall static pressure. It proceeds from the results that the pressure recovery and combustion efficiency can be predicted confidently from the simulation. These computations also confirmed that for the specific injected design investigated, the combustion efficiency is limited by an imperfect mixing between fuel and air. Manna et al. [20] have numerically explored the effect of the combustor inlet Mach number and total pressure on the flow development in the scramjet combustor. It has been shown that higher combustor entry Mach number and distributed fuel injection are required to obtain predominant supersonic flow and avoid thermal choking. The presence of fuel injection struts make the flow fully three-dimensional, cause significant flow blockage and affect the mixing and combustion pattern in the scramjet combustor. Mixing and combustion issues in a small sized combustor are markedly different than that of a flight-sized combustor. Detailed numerical simulations of strut-based flight-sized kerosene fuelled scramjet combustor are not reported adequately in the literature.

Pannervselvam et al. [25] have presented a hypersonic cruise air-breathing mission with airframe integrated scramjet engine. The design and performance parameters of various individual components like forebody, intake, combustor and nozzle were presented based on a generalized steady quasi one-dimensional flow model. In this work, three-dimensional viscous simulations are presented for a full scale flight module scramjet combustor for hypersonic air breathing mission with kerosene fuel injected from a row of struts placed in the flow path. Thermochemical parameters are analysed to estimate the flow behavior in the combustor. The effects of middle wall, redistribution of fuel within the struts, relocation of struts and fuel droplet size distribution on the performance of the combustor are presented.

## 2. Combustor and computational details

A typical cruise hypersonic air-breathing mission has been explained in Ref. [25] for the demonstration of 20 seconds duration flight. The operating Mach number and altitudes are 6.5 and 32.5 km respectively. Due to the limitation of the connected pipe mode test facility, the development and testing of the scramjet combustor was focused on the half scale module. The full scale combustor has been made half by putting a wall at the mid-width of the combustor. The combustor has an entry cross section of  $H_i \times W_i$  ( $H_i = 0.05L$ ,  $W_i = 0.3L$ ,  $L$  being the length of the combustor), exit cross section  $H_{out} \times W_{out}$  ( $H_o = 0.14L$ ,  $W_{out} = W_i = 0.3L$ ). The width of the combustor is kept constant throughout the length. However, the height of the combustor is varied while ascertaining that the combustor can be fitted in the overall vehicle envelope without much drag penalty.

The schematic of the scramjet combustor and 3D view are shown in Figs. 1a and 1b respectively. The combustor has four sections. The 1st section has a constant area with a length  $0.05L$ , followed by  $1^\circ$  divergent (2nd section) for  $0.11L$  length,  $4^\circ$  divergent (3rd section) for  $0.4L$  length and finally  $7.5^\circ$  divergent (4th section) of  $0.44L$  length. A middle wall with a thickness of  $0.01L$  has been placed at a distance of  $0.14L$  from the inlet connecting the top and bottom wall of the combustor. The middle wall has a wedge of  $12^\circ$  at the leading edge. Kerosene fuel is injected through 220 injection holes (with 0.5 mm diameter for each hole) provided through 10 struts. Each strut has 11 injection holes on either side and has equal fuel distribution through each injection hole. The

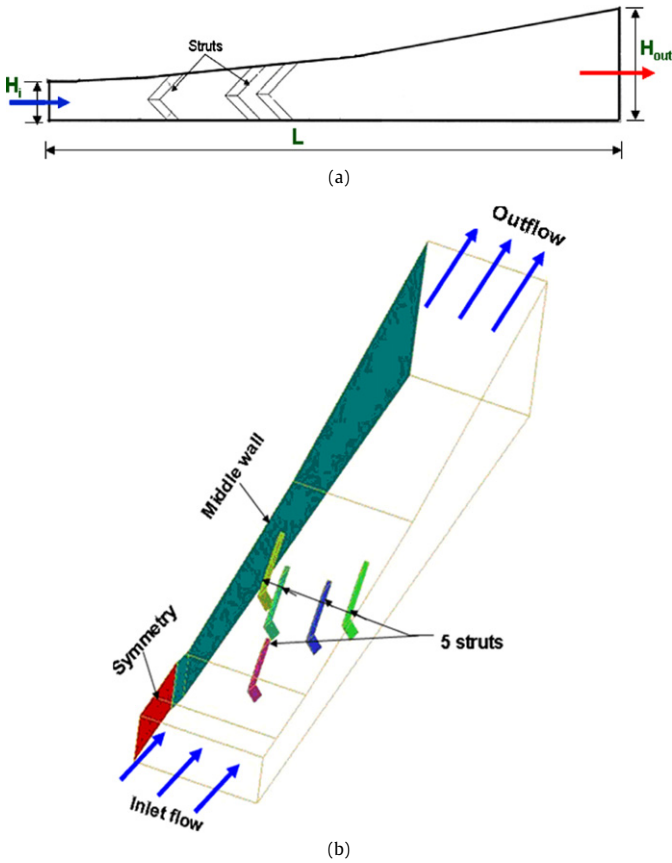


Fig. 1. (a) Schematic of the scramjet combustor (baseline). (b) 3D view of the scramjet combustor (half geometry).

schematic of typical strut geometry is shown in Fig. 2. The cross-section from the leading edge is sweeping backwards in the upper and lower parts. Marquardt Corporation, USA [21] has investigated this sweptback type of strut in scramjet combustor to increase the three-dimensionality of the flow. Leading edges with small radius and blunt trailing edges have been provided in the strut to keep the shock attached and flame holding purpose respectively.

Pure air is considered at the entry of the combustor as it is supposed to provide the thrust to a hypersonic flight vehicle flying at a speed of about 6.5 Mach and altitude of 32.5 km [25], corresponding to which the combustor entry Mach number is 2.0 approximately

### 3. Computational methodology

Three-dimensional Reynolds Averaged Navier Stokes (RANS) equations are solved using CFX-code [5], which is an integrated software system capable of solving diverse and complex multidimensional fluid flow problems. The code is fully implicit, finite volume method with finite element based discretization of geometry. The method retains much of the geometric flexibility of finite element methods as well as the important conservation properties of the finite volume method. It utilizes numerical upwind schemes to ensure global convergence of mass, momentum, energy and species. It implements a general non-orthogonal, structured, boundary fitted grids. To circumvent the initial numerical transient, the discretization of the convective terms are done by first order upwind difference scheme till few time steps initially and subsequently, the convective terms are discretized through 2nd order scheme to capture the flow features more accurately. The turbulence model used was  $k-\epsilon$  model with wall functions.

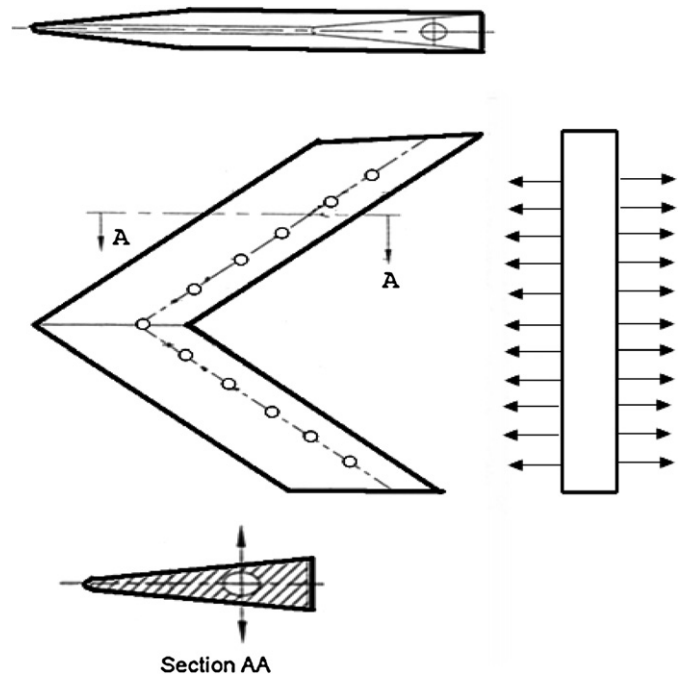
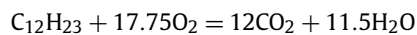


Fig. 2. Typical strut geometry.

For combustion, the eddy dissipation combustion model is used for its simplicity and robustness in predicting the performance of reactive flows in many engineering applications. The eddy dissipation model is based on the concept that chemical reaction is fast compared to the transport process in the flow. When reactants mix at the molecular level, they instantaneously form products. The model assumes that the reaction rate may be related directly to the time required to mix reactants at molecular level. In turbulent flows, this mixing time is dictated by the eddy properties and therefore the burning rate is proportional to the rate at which turbulent kinetic energy is dissipated, i.e., reaction rate is proportional to  $\epsilon/k$ , where  $k$  is the turbulent kinetic energy and  $\epsilon$  is its rate of dissipation. The chemistry of the kerosene ( $C_{12}H_{23}$ ) reaction is represented on a molar basis by,



The mixing rate determined from the EDM is given as

$$R_{k,EDM} = -A_{ebu}\rho\frac{\epsilon}{k}\min\left\{y_f, \frac{y_{ox}}{r_k}, B_{ebu}\frac{y_p}{1+r_k}\right\}$$

Here,  $\rho$  and  $y_f$ ,  $y_{ox}$  and  $y_p$  are the density and mass fractions of fuel, oxidizer and products respectively,  $A_{ebu}$  and  $B_{ebu}$  are the model constants and  $r_k$  is the stoichiometric ratio.

Lagrangian Particle Tracking Method is used for discrete phase model to characterize the flow behavior of the dispersed phase fluid (kerosene liquid) along with the flow of the continuous phase predicted using a discretized form of the RANS equations. Solutions are marched with global time step typically at  $10^{-5}$  s. Log-normalized maximum residue of  $-04$  is considered as the convergence criteria.

The software is thoroughly validated for a number of applications pertaining to the combustion of hydrogen and kerosene fuel with supersonic air flow in the scramjet combustor including transverse  $H_2$  injection in a constant area duct [18], staged  $H_2$  injection from struts [29], pylon injectors [13], kerosene fuelled scramjet combustor with cavity injector [19] and ramp-cavity based injector [26]. All these works revealed that although, there are some differences in the near injection zones, both the computational and experimental results match well within the 5% in

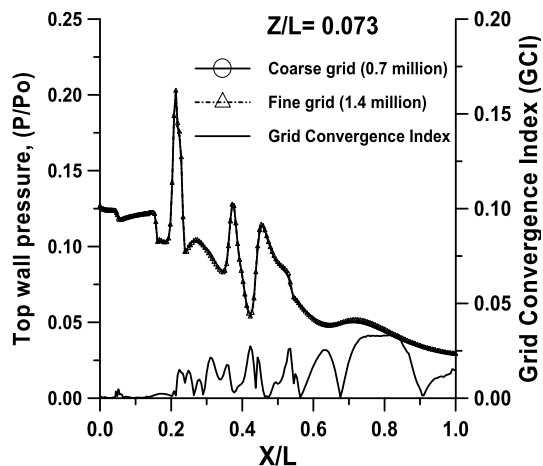


Fig. 3. Top wall surface pressure comparison with two different grids.

the diverging combustor where major thrust for the combustor is produced.

#### 4. Results and discussion

Since there is symmetry along the width of the combustor, half of the combustor is considered for computational domain. In the analysis,  $X$ -axis is taken along the combustor length, while,  $Y$ -axis and  $Z$ -axis are considered along the height and the width of the combustor. The origin for the co-ordinate system is placed at the middle of the bottom wall at combustor entry. Initial  $0.14L$  from the combustor inlet upto the starting of the middle wall has been considered as symmetry. All the flow properties are kept constant in the inflow plane, as the inflow boundary is supersonic. No slip and adiabatic wall boundary conditions are imposed on all the walls while symmetry condition is prescribed in the symmetry plane. Supersonic outflow boundary condition has been applied at the exit of the computational domain.

Multiblock structured grid has been generated [2] for the whole geometry. Grids are clustered towards the walls and around the struts to capture the high gradient reacting flows. Grids of size about  $250 \times 62 \times 48$  (0.7 million) grid points have been generated for the computational domain. A minimum  $y^+$  of 13.6 is used for all the no slip walls. Adjacent to the injection point, the original grids are made finer by 4–8 times by grid embedding to capture the very small injection holes. The grid independence of the results is demonstrated by comparing the nonreacting flow simulation in the baseline configuration with two different grids namely 0.7 million and 1.4 million. The grid is made more than doubled in the fuel injection zone where gradients are expected to be high. In the divergent portion of the combustor, where the flow development is relatively smooth the grid has not been changed significantly. The top wall surface pressures at  $Z/L = 0.073$  for two different grid are compared in Fig. 3 and a very good comparison is obtained. An estimate of the error due to grid in the form of Grid Convergence Index (GCI) is also presented in the figure. For steady state boundary-value problem, the main source of numerical error in CFD is iterative convergence or grid convergence error. This error can be estimated by running the solution in two different grids (coarse and fine). The simplest of such estimate is given by the relative difference  $\epsilon = (f_2 - f_1)/f_1$  [7], where  $f$  represent any quantity of interest and the indices 1 and 2 refer to the fine and coarse grid solution respectively. (In the present calculation, surface pressure has been taken as the parameter of interest.) Roache

[28] has proposed a grid convergence index (GCI) as an error based on uncertainty estimate of the numerical solution as

$$GCI = F_s \frac{1 \in 1}{(h_2/h_1)^p - 1}$$

Here,  $h$  is the order of grid spacing,  $p$  is the order of accuracy of numerical scheme and  $F_s$  is a factor of safety. Roache [27] has suggested  $F_s = 3$  for minimal of two grid calculations. For the present calculation  $p$  is equal 2 with  $h_2/h_1$  equal to 2, GCI is order of  $\epsilon$ . Maximum error between two simulations is within 3.33%. This analysis indicates that the grid is adequate to capture most of features of the flow and the solution in grid independent.

The numerical simulations are made to study the effect of the followings on the performance of the combustor and compared with the baseline configuration

- (i) Combustor without middle wall – Case-1;
- (ii) Redistribution of fuel – Case-2;
- (iii) Re-location of struts – Case-3;
- (iv) Rosin–Rammler fuel droplet distribution – Case-4.

Reacting flow simulations have been carried out for the kerosene fuel injection with an equivalence ratio ( $\phi$ ) of 1.0. Kerosene is injected (through a number of injection holes of 0.5 mm diameter each placed in the struts as shown in Fig. 2) transversely into the supersonic air stream. Yu et al. [35] measured the droplet distribution of kerosene fuel in supersonic stream and reported kerosene SMD (Sauter Mean Diameter) of  $20 \mu\text{m}$  for 20–25 bar of injection pressure. In absence of actual droplet distribution data for the given flow condition, the data reported by Yu et al. [35] is used in the simulation. Injection velocity is estimated from the pressure difference between the upstream and downstream across the injector orifice. Injector discharge coefficient is taken as 0.63. Injection velocity 45.0 m/s and temperature of 300 K are considered for the kerosene inflow conditions for all the cases except Case-4.

##### 4.1. Baseline configuration (combustor-1)

The pattern of liquid kerosene fuel injection and vaporization has been shown in Fig. 4. 20% of the total fuel has been injected from 1st strut which is located at the mid-width of the half combustor at an axial location between  $X/L = 0.18$  and  $0.24$ . Remaining 80% of the total is injected from 2nd (two nos) and 3rd (two nos) group of struts which are located at  $X/L = 0.031$  to  $0.44$ . Liquid kerosene emerges from the injection holes transversely with the main flow in the form of droplets and interacts with the high speed and high temperature airflow. Due to the heat and mass transfer with the air particle, the bigger drops of fuel break into smaller drops, vaporizes and finally take part in the reaction process with the oxygen available in the air. The process of the vaporization is slow; however, it is completed within the available length of the combustor for the total amount of kerosene. Though the fuel injection is completed at  $X/L = 0.44$ , the vaporization process is almost complete at about  $X/L = 0.63$ .

The Mach number distribution at different cross sectional planes ( $X/L = 0.0, 0.11, 0.22, 0.33, 0.44, 0.55, 0.71, 0.87$  &  $1.0$ ) is shown in Fig. 5 in supersonic scale. Clearly the flow has become almost subsonic behind the struts due to reaction. Area averaged Mach number (shown in Fig. 19) has become subsonic between  $0.29 < X/L < 0.50$  with the minimum subsonic Mach number of 0.74 reaching at about  $X/L = 0.38$ . The static pressure (non-dimensionalized with combustor inlet total pressure,  $P_o$ ) and static temperature (non-dimensionalized with combustor inlet total temperature,  $T_o$ ) distributions at different axial locations ( $X/L = 0.0,$

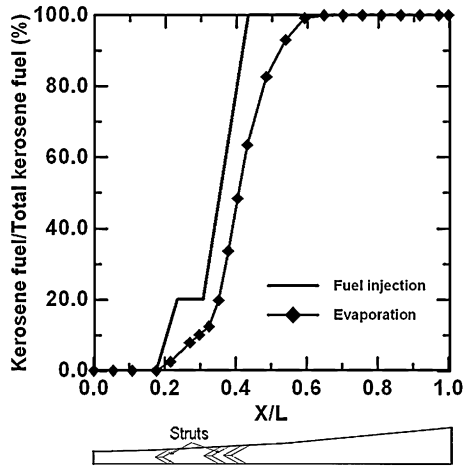


Fig. 4. Fuel injection and vaporization pattern along the length.

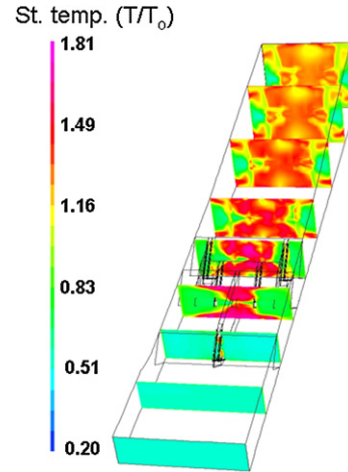


Fig. 7. Static temperature contours at various axial locations.

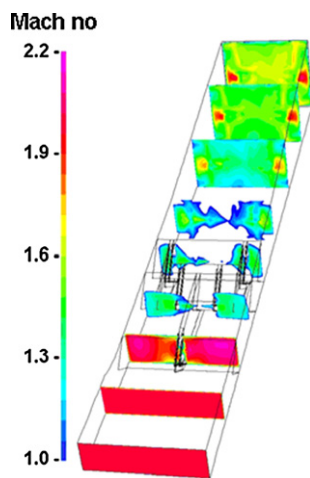


Fig. 5. Mach number contours at various axial locations.

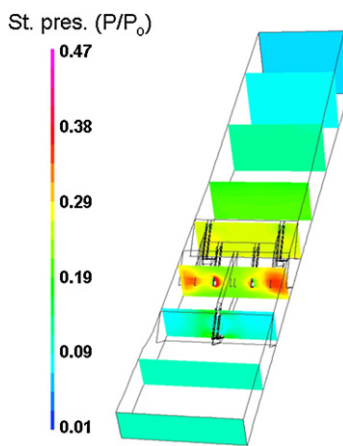


Fig. 6. Static pressure contours at various axial locations.

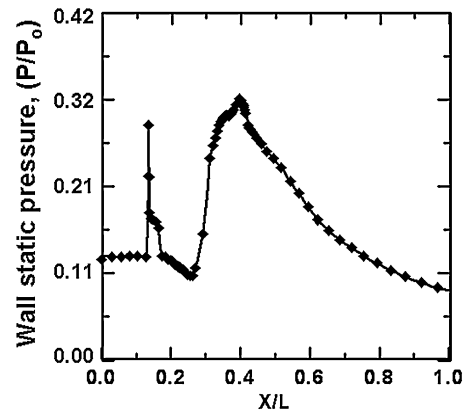


Fig. 8. Top wall pressure distribution at  $Z/W = 0$ .

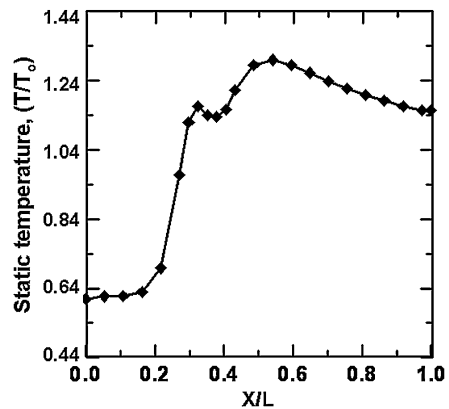


Fig. 9. Area averaged static temperature distribution.

0.11, 0.22, 0.33, 0.44, 0.55, 0.71, 0.87 & 1.0) are shown in Figs. 6 and 7 respectively.

The rise of pressure and temperature in the combustion region (adjacent to the struts) of the combustor is due to reaction of kerosene fuel, whereas, in the later part (divergent section) the pressure and temperature slowly decrease due to the expansion of flow.

The top wall static pressure on combustor at mid-width plane is shown in Fig. 8. The sudden pressure rise (1st peak) at around

$X/L = 0.14$  is due to shock generated from the wedge of middle wall. The 2nd peak of pressure regions is generated due to the combustion of kerosene fuel. The pressure values gradually decrease in the divergent section towards the exit of the combustor. The average non-dimensionalized pressure is 0.09 at the exit of the combustor. The average static temperature distribution is shown in Fig. 9. Due to the reaction of fuel injected from the first strut, temperature increases upto  $X/L = 0.31$  where, 2nd struts fuel injection starts. Due to the vaporization and mixing of the fuel injected (80% of the total fuel) from 2nd and 3rd group of struts, average temperature decreases from  $X/L = 0.31$  to 0.38. After that due to reaction of these fuels temperature starts rising and reaches maximum at

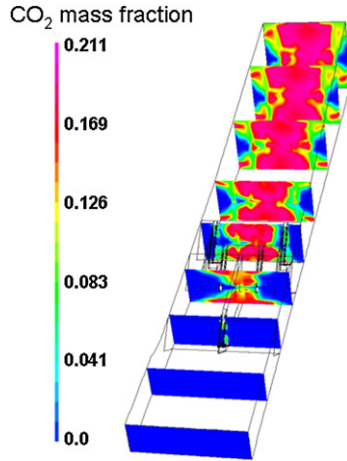


Fig. 10. CO<sub>2</sub> mass fraction at various axial locations.

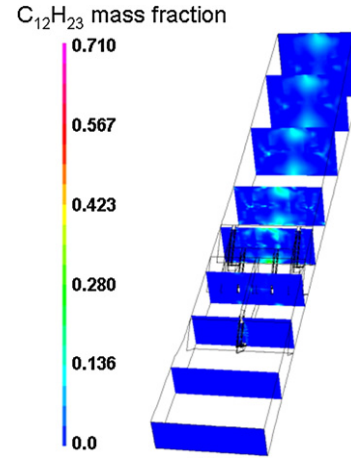


Fig. 12. C<sub>12</sub>H<sub>23</sub> mass fraction at various axial locations.

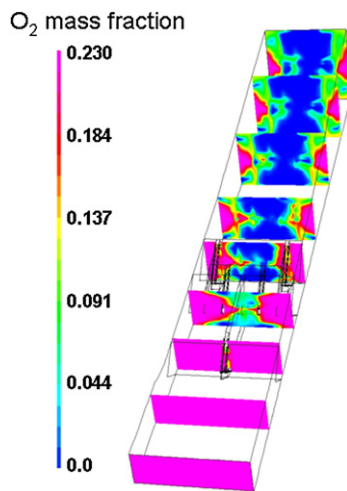


Fig. 11. O<sub>2</sub> mass fraction at various axial locations.

about  $X/L = 0.54$  and then decreases slowly due to the expansion of the flow.

The mass fractions of CO<sub>2</sub>, O<sub>2</sub> and kerosene vapor at various axial stations ( $X/L = 0.0, 0.11, 0.22, 0.33, 0.44, 0.55, 0.71, 0.87$  &  $1.0$ ) have been shown in Figs. 10, 11 and 12 respectively. Increase in CO<sub>2</sub> (Fig. 10) and decrease of O<sub>2</sub> (Fig. 11) in the core region of the combustor depict that the combustion of kerosene has occurred mostly in the core region of the combustor. Lot of unused oxygen is available towards the middle and side wall regions of the combustor, whereas, considerable amount of unburnt kerosene vapor has been found (Fig. 12) in the core region of the combustor.

The amount of burnt and un-burnt kerosene vapor has been shown in Fig. 13. Almost 31% of total kerosene injected remains un-burnt at the exit of the combustor. This indicates that a better distribution of fuel can improve the performance of the combustor. The combustion efficiency is defined as the ratio of the amount of kerosene burnt to the total amount of kerosene injected into the combustor. The combustion efficiency and the thrust available per unit fuel rate from the combustor are about 69.0% (as shown in Fig. 20) and 5867.4 N respectively.

#### 4.2. Case-1: Baseline configuration without middle wall

To see the effect of the middle wall on the combustor performance, a separate numerical analysis has been carried out by removing the middle wall from the combustor (named as combustor-2). In the simulation, a symmetric plane has been con-

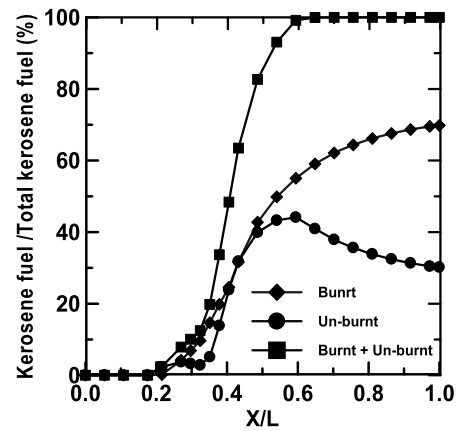


Fig. 13. Fuel consumption characteristics.

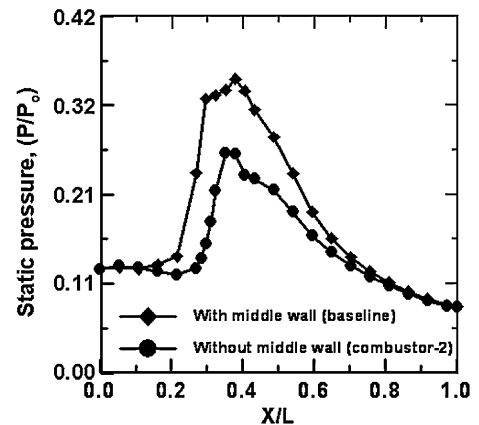


Fig. 14. Area averaged static pressure comparison.

sidered in place middle wall of the combustor. All other geometrical and inflow parameters remain the same as the baseline configuration. The results of the area average static pressure (Fig. 14) and the Mach number (Fig. 19) are compared with the baseline configuration. Comparatively lesser rise in static pressure as well as lesser decrease in Mach number have been found in combustor-2 compared to the baseline combustor which is due to the less amount kerosene burnt in combustor-2. In fact, the presence of middle wall has enhanced the mixing and the combustion of kerosene fuel with the supersonic air flow inside the combustor. The combustion efficiency has been found to be about 64.0%

**Table 1**  
Comparison of various fuel injection schemes.

	Number of injection holes				
	Strut-1R	Strut-2R-L	Strut-2R-R	Strut-3R-L	Strut-3R-R
Baseline combustor	11(L) + 11(R)	11(L) + 11(R)	11(L) + 11(R)	11(L) + 11(R)	11(L) + 11(R)
Case-2	11(L) + 11(R)	11(L) + 07(R)	07(L) + 11(R)	14(L) + 12(R)	12(L) + 14(R)

**Table 2**  
Description of strut position within the combustor.

	Location	Strut-1R	Strut-2R-L	Strut-2R-R	Strut-3R-L	Strut-3R-R
Baseline combustor	Z/H <sub>i</sub>	1.64	1.10	2.19	0.55	2.74
Case-3	Z/H <sub>i</sub>	1.64	1.03	2.26	0.41	2.88

compared to 69.0% in the baseline configuration. The achieved net thrust per unit fuel flow rate is 5605.7 N which is 4.5% lesser than that of the baseline configuration. The combustor with middle wall (combustor-1) has been considered for the further study to improve the performance of the combustor in terms of combustion efficiency and net thrust availability.

#### 4.3. Case-2: Baseline combustor with redistribution of fuel injection

As mentioned earlier that a better fuel distribution is required for better fuel–air mixing and combustion and hence to decrease the amount of un-burnt kerosene vapor from the core region. The distribution of un-burnt kerosene vapor in the baseline combustor is analyzed in detail and the change in fuel distribution scheme has been decided. The modified fuel injection scheme in comparison to baseline fuel injection scheme is provided in Table 1 (for half geometry), where L and R represent left and right side of the struts (looking from the entry plane). It can be seen from the table that excess fuel from the core side of strut-2 (pair) has been withdrawn and redistributed towards the wall side regions of strut-3 (pair). With the new fuel injection locations a new simulation is carried out keeping all the boundary conditions same and the performance parameters are calculated. The combustion efficiency and the thrust per unit fuel flow rate have been achieved 74.1% and 6259.7 N respectively. Hence the combustion efficiency and net thrust have been found to 7.4% and 6.6% more compare to the baseline configuration.

#### 4.4. Case-3: Baseline combustor with redistribution of fuel injection and relocation of struts

In this case, in addition to the modifications of fuel distribution (as discussed above in Case-2), the positions of the strut locations along the combustor width have been changed while the position of the struts along the axial locations of the combustor kept the same as compared to baseline combustor. The new location of the struts of the present case has been presented in Table 2 along with the baseline combustor. With the new strut locations and modified fuel injection locations (Case-2), a new simulation is carried out and combustor performance parameters are calculated. The combustion efficiency is increased about 10.7% while the net thrust availability is improved about 8.8% compared to the baseline configuration.

#### 4.5. Case-4: Rosin Rammler fuel droplet distribution

In all the previous cases, the kerosene fuel droplet size is taken a constant value of droplet diameter = 20 μm. However, in actual, droplets coming from an injector contain a distribution of wide ranges from very fine (~ 1 μm) to coarse (~ 120 μm) droplet sizes. Coarser droplets require larger length of combustor for its vapor-

ization, hence, complete combustion. Various fuel droplets can be represented with Rosin–Rammler distribution [16] as follows:

$$R_c = \exp[-(D/D_e)^\gamma]$$

Here,

$R_c$  = cumulative mass fraction above a given particle diameter  $D$ ,  
 $D_e$  = measure of fineness and equal to the diameter at which  $R_c = 0.368$  and  
 $\gamma$  = measure of size dispersion, a lower value indicates wide distribution.

The numerical simulation has been carried out for the baseline combustor with relocated strut and modified fuel injection system (Case-3) keeping the inflow boundary conditions for supersonic air and liquid kerosene identical as the previous cases. However, the distribution of kerosene droplet diameter varies. In the present study, a Rosin–Rammler distribution of particle sizes of  $D_e = 37.32 \mu\text{m}$  and  $\gamma = 1.5$  (equivalent SMD = 13.93 μm) has been taken for the simulation. For this, distribution of various mass fractions with particle size is shown in Fig. 15.

The comparison of CO<sub>2</sub> mass fraction for Cases-3 and 4 at exit plane of the combustor is shown in Fig. 16. It is clear, that combustion is more uniform in the Case-4 compared to Case-3. Typical particle trajectory between Case-3 and Case-4 from 3R strut is shown in Fig. 17. It can be seen that the droplet from RR distribution takes much longer time to evaporate. The penetration of the fuel towards the wall seems to be more for Case-4 compared to Case-3. This has caused better consumption of O<sub>2</sub> resulting in more uniform CO<sub>2</sub> mass fraction at the exit of the combustor.

The kerosene fuel injection and reaction characteristics along the length of the combustor are shown in Fig. 18. It can be seen that the unburnt and burnt kerosene vapor almost amounts to the total liquid kerosene injected. Hence, the kerosene leaving the combustor in liquid form is negligible.

The comparison of area averaged Mach number and combustion efficiency for baseline configuration with all four cases are presented in Figs. 19 and 20 respectively.

The combustion characteristics along the length of the combustor reveals that the combustion fuel in the baseline combustor is more which makes the subsonic Mach number lower than the other cases in the reaction intense zone. For the other cases (except Case-1), combustion increases slowly which shows the combustion is smooth along the length of the combustor. The maximum combustion efficiency has been achieved 81.6% in baseline combustor with modified fuel distribution and strut locations and with various particle distributions. The combustion efficiency and net thrust have been improved to 18.3% and 18.6% respectively compare to the baseline configuration. Because of the change of the fuel distribution from a constant particle size of 20 μm to Rosin–Rammler particle distribution, combustion efficiency and

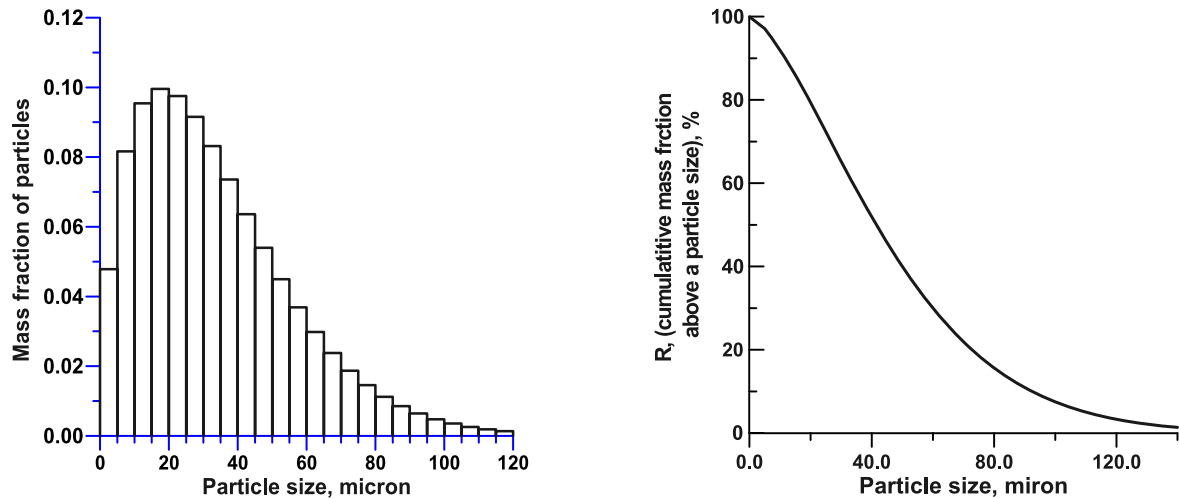


Fig. 15. Droplet distribution for  $D_e = 37.32\mu\text{m}$  and  $\gamma = 1.5$ .

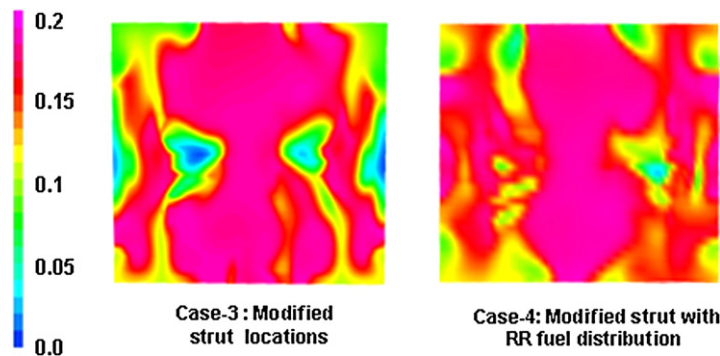


Fig. 16. Comparison of  $\text{CO}_2$  mass fraction.

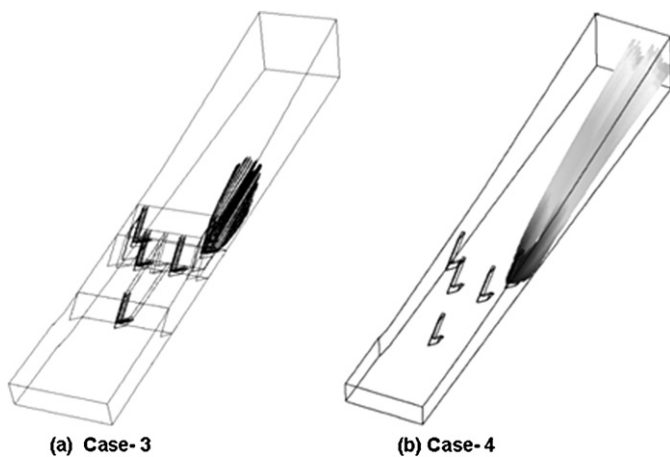


Fig. 17. Comparison of  $\text{C}_{12}\text{H}_{23}$  liquid trajectory.

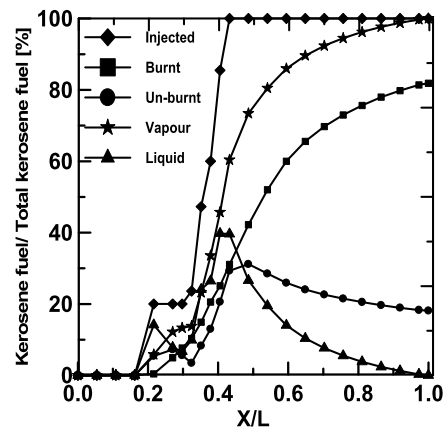


Fig. 18. Comparison of kerosene flow behaviors in combustor.

thrust have been improved by 6.8% and 9.1% respectively. The comparison of combustor performance in terms of combustion efficiency and thrust for all the cases including the baseline combustor has been presented in Table 3.

### 5. Conclusions

A flight sized scramjet combustor is optimized for thrust and combustion efficiency using CFD tools. 3-D RANS equations along with  $k-\epsilon$  turbulence model are solved. The effect of middle wall on the combustor performance is evaluated by comparing simula-

tion results. Middle wall is seen to improve mixing between fuel and air. Combustor Performance is optimized by redistributing the fuel (Case-2) and relocating the strut (Case-3). It is observed that the combustor with relocated strut having modified fuel injection scheme has the maximum performance. Consideration of proper drop size distribution (Case-4) is seen to have significant effect on combustor performance. It is observed that almost all droplets including large drops ( $\sim 50\text{--}120$  micron) present in the distribution are completely evaporating and kerosene leaving combustor in liquid form is negligible. The combustor with relocated strut (Case-3) is the best configuration and is found to give maximum performance with the drop size distribution (Case-4).

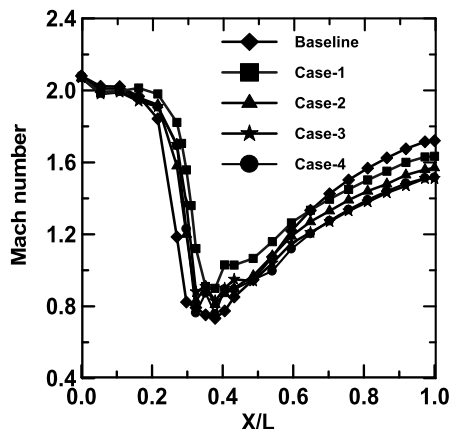


Fig. 19. Comparison of area averaged Mach number.

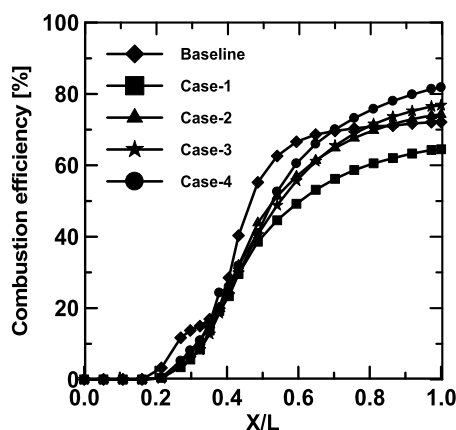


Fig. 20. Comparison of combustion efficiency.

**Table 3**  
Comparison of performance with baseline combustor.

Cases	Combustion efficiency, $\eta$ (%)	Increase in $\eta$ (%)	Thrust per unit fuel flow rate (N)	Increase in thrust (%)
Baseline combustor	69.0	–	5870.4	–
Case-1	64.0	(–)7.2	5605.7	(–)4.5
Case-2	74.1	7.4	6259.7	6.6
Case-3	76.4	10.7	6384.3	8.8
Case-4	81.6	18.3	6965.1	18.6

**Acknowledgements**

The authors are thankful to Dr. V. Ramanujachari and his team for their valuable suggestions during the course of work. We sincerely acknowledged the support provided for the preparation of the combustor geometry and finalization of flow conditions.

**References**

[1] J.D. Abblit, R.J. Hartfield, J.C. McDaniel, Mole fraction imaging of transverse injection in a ducted supersonic flow, *AIAA Journal* 29 (3) (1991) 431–435.  
 [2] ANSYS ICEM-CFD-11, Installation and overview, January-2007.  
 [3] M. Bouchez, E. Dufour, X. Montazel, Hydrocarbon fueled scramjet for hypersonic vehicles, *AIAA paper No. 1998-1589*, 1998.  
 [4] R. Burnes, T.P. Parr, K.J. Wilson, K. Yu, Investigation of supersonic mixing control using cavities – effects of fuel injection location, *AIAA paper No. 2000-3618*, 2000.  
 [5] CFX Computational Fluid Dynamics, Software Version 2.11.1, AEA Technology Engineering Software Ltd., 2001.

[6] E.T. Curran, Scramjet engines: The first forty years, *Journal of Propulsion and Power* 17 (6) (2001) 1138–1148.  
 [7] A.D. Cutler, P.M. Danehy, S. O’Byrne, C.G. Rodrigues, J.P. Drummond, Supersonic combustion experiment for CFD model development and validation, *AIAA paper No. 2004-266*, 2004.  
 [8] E. Dufour, M. Bouchez, Computational analysis of a kerosene fueled scramjet, *AIAA paper No. 2001-1817*, 2001.  
 [9] A.K. Edward, A.S. Joseph, Liquid jet injection into a supersonic flow, *AIAA Journal* 11 (9) (1973) 123–1224.  
 [10] A. Feri, Review of problems in application of supersonic combustion, *Journal of Royal Aeronautical Society* 68 (645) (1964) 575–597.  
 [11] M.R. Gruber, J.M. Donbar, C.D. Carter, K.Y. Hsu, Mixing and combustion studies using cavity-based flame holders in a supersonic flow, *Journal of Propulsion and Power* 20 (5) (2004) 769–778.  
 [12] K.Y. Hsu, C. Carter, J. Crafton, M. Gruber, J. Donbar, T. Mathur, D. Schommer, W. Terry, Fuel distribution about a cavity flame-holder in supersonic flow, *AIAA paper No. 2000-3585*, 2000.  
 [13] Afroz Javed, Debasis Chakraborty, Numerical simulation of supersonic combustion of pylon injected hydrogen fuel in scramjet combustor, *Journal of Institution of Engineers* 87 (2006) 1–6.  
 [14] T. Kanda, T. Hiraiwa, T. Mitani, S. Tomioka, N. Chinzei, Mach 6 testing of a scramjet engine model, *Journal of Propulsion and Power* 13 (4) (1997) 543–551.  
 [15] T. Kanda, T. Sunami, S. Tomioka, K. Tani, T. Mitani, Mach 8 testing of scramjet engine model, *Journal of Propulsion and Power* 17 (1) (2001) 132–138.  
 [16] Kenneth K. Kuo, *Principles of Combustion*, Wiley-Interscience Publications, 1986.  
 [17] J.G. Li, G. Yu, X.Y. Zhang, Q.S. Huang, Combustion of kerosene in a supersonic stream, *AIAA paper No. 2000-0615*, 2000.  
 [18] P. Manna, Debasis Chakraborty, Numerical simulation of transverse H<sub>2</sub> combustion in supersonic airstream in a constant area duct, *Journal of Institution of Engineers* 86 (2005) 47–53.  
 [19] P. Manna, Behera Ramesh, Debasis Chakraborty, Thermochemical exploration of a cavity based supersonic combustor with liquid kerosene fuel, *Journal of Aerospace Sciences and Technologies* 59 (4) (2007) 246–258.  
 [20] P. Manna, Behera Ramesh, Debasis Chakraborty, Liquid fueled strut based scramjet combustor design – a computational fluid dynamics approach, *Journal of Propulsion and Power* 24 (2) (2008) 274–281.  
 [21] Marquardt Corporation, Supersonic combustion tests in an 8000 FPS air stream, Report No. 6064, VAN NUYS, California, USA, 1964.  
 [22] T. Mathur, M. Gruber, K. Jackson, J. Donbar, W. Donaldson, T. Jackson, F. Billig, Supersonic combustion experiments with a cavity-based fuel injector, *Journal of Propulsion and Power* 17 (6) (2001) 1305–1312.  
 [23] H. Miyajima, N. Chinzei, T. Mitani, Y. Wakamatsur, M. Maita, Development status of the NAL scramjet engine test facility and subscale scramjet engine, *AIAA paper No. 92-5094*, 1992.  
 [24] G.B. Northam, G.Y. Anderson, Supersonic combustion ramjet research at Langley, *AIAA paper No. 86-0159*, 1986.  
 [25] S. Pannerselvam, V. Thiagarajan, A.T.K. Ganesh, J.J. Geetha, V. Ramanujachari, Pahlada, Airframe integrated scramjet design and performance analysis, *ISABE paper No. 2005-1280*, 2005.  
 [26] Behera Ramesh, Debasis Chakraborty, Numerical simulation of kerosene fueled ramp cavity based scramjet combustor, *Journal of Aerospace Sciences and Technologies* 58 (2) (2006) 104–112.  
 [27] P.J. Roache, *Verification and Validation in computational Science and Engineering*, Hermon Publishers, New Mexico, 1998.  
 [28] P.J. Roache, Error bars for CFD, *AIAA paper No. 2003-0408*, 2003.  
 [29] Saha Soumyajit, Chakraborty Debasis, Reacting flow computation of staged supersonic combustor with strut injection, in: *Proceedings of 36th AIAA Fluid Dynamics Conference*, San Francisco, USA, 2006, *AIAA paper No. 2006-3895*.  
 [30] T. Sunami, N. Sakuranaka, K. Tani, T. Kiraiwa, T. Shimura, Mach 4 test of a scramjet engine – effect of isolator, in: *Proceeding of 13th International Symposium of Air Breathing Engine*, AIAA, Washington, DC, 1997, pp. 615–625.  
 [31] V.A. Vinogradov, S.A. Kobigsky, M.D. Petrov, Experimental investigation of kerosene fuel combustion in supersonic flow, *Journal of Propulsion and Power* 11 (1) (1995) 130–134.  
 [32] P.J. Waltrup, Liquid-fueled supersonic combustion ramjet: A research perspective, *Journal of Propulsion and Power* 3 (6) (1987) 515–524.  
 [33] K. Yokota, S. Kaji, Two and three dimensional study on supersonic flow and mixing fields with hydrogen injection, *AIAA paper No. 95-6024*, 1995.  
 [34] G. Yu, J.G. Li, X.Y. Chang, L.H. Chen, C.J. Sung, Fuel injection and flame stabilization in liquid – kerosene fueled supersonic combustor, *Journal of Propulsion and Power* 19 (5) (2003) 885–893.  
 [35] K.H. Yu, K.J. Wilson, K.C. Schadow, Effect of flame holding on supersonic – combustion performance, *Journal of Propulsion and Power* 17 (6) (2001) 1287–1295.